Screening Current-Induced Stress and Strain Analysis Considering a Non-uniform Thickness Profile of REBCO Tapes

Yu Suetomi, Shannon Griffin, Hongyu Bai, Mark Bird, *Senior Member, IEEE*, Dmytro Abraimov, *Member, IEEE*, Adonay Almanza-Enriquez, Noah Gavin, Jun Lu, and Iain R. Dixon, *Senior Member, IEEE*

***Abstract*—Winding compressibility (WCP) is a significant reduction in the effective radial Young's modulus of REBCO pancake coils compared with the sum of the various macroscopic components, due to microscopic asperities on the tape surface and/or a non-uniform tape profile. For pancakes that are impregnated either not at all or with something soft like paraffin, this has a substantial impact on the screening current induced stress (SCIS) calculation. In this study, we propose a modeling technique called Penalty Function with Gap Offset (PGO) that incorporates non-uniform tape profiles as a gap offset distribution within contact boundaries. We also evaluate the effectiveness of reinforcement options—co-winding (CW), over-banding (OB), and outer ring (OR)— by considering winding compressibility.**

***Index Terms*—Coupled mechanical and electromagnetic analysis, REBCO coil, screening current induced stress, ultra-high field superconducting magnet, winding compressibility.**

I. Introduction

STRESS and strain management considering screening current induced stress (SCIS) is crucial in designing ultra-high field (UHF) solenoids using REBCO tapes. The screening current in REBCO tapes generates both outward and inward Lorentz forces, resulting in conical deformation of the REBCO pancake coil, increased tensile hoop strain, and the emergence of compressive hoop strain [1], [2], [3], [4].

To address these effects, we developed a numerical simulation tool to calculate SCIS and evaluated the effectiveness of reinforcement techniques such as co-winding and over-banding with stainless-steel tape [5], [6], [7]. However, these studies did not consider the winding compressibility, that has recently gained increased attention.

As illustrated in Fig. 1, winding compressibility is caused by microscopic asperities and/or non-uniform tape profiles. This leads to compression of the winding pack, significantly reducing the effective radial Young's modulus of the winding pack $E_{\mathrm{r,eff}}$ and introducing nonlinear stress-strain behavior [8], [9]. These characteristics have been observed in REBCO tape stacks [10], [11] and pancake coils [8], [12]. The $E_{\mathrm{r,eff}}$ values estimated from the measured stress-strain curves of REBCO tape stacks range from 1.50–2.35 GPa at 20–40 MPa of compression stress and 2.63–4.64 GPa at 80–100 MPa [11], which are approximately two orders of magnitude lower than the Young's modulus of the REBCO tape. This discrepancy significantly affects structural analysis results.

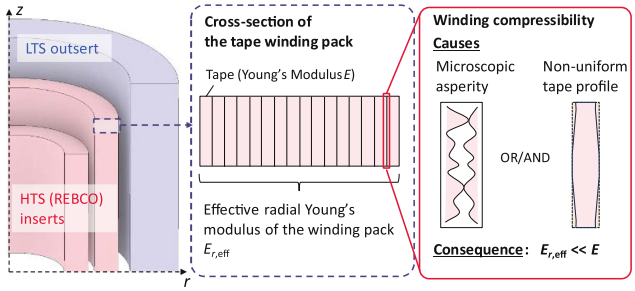

Fig. 1. Schematic illustration of the causes and consequence of winding compressibility.

A method for incorporating the nonlinear stress-strain behavior into structural FEM models was proposed in [9], using a nonlinear contact pressure function derived from an experimental stress-strain curve of REBCO tape stacks and implemented as a penalty function at the contact boundary. However, this approach does not account for non-uniformity across the tape width.

In this study, we propose a modeling technique that incorporates the non-uniform tape profile, and re-evaluates the effectiveness of reinforcement, taking winding compressibility into account.

II. Modeling Approach

A. Penalty Function With Gap Offset (PGO)

Although REBCO tapes typically exhibit a "dog-bone" shape—where the edges are thicker than the center—due to the copper electroplating process [13], some recent REBCO tapes

Received 28 July 2025; revised 28 October 2025; accepted 16 November 2025. Date of publication 26 November 2025; date of current version 9 December 2025. This work was supported in part by the National High Magnetic Field Laboratory, in part by the National Science Foundation under Cooperative Agreement DMR-2131790 and Cooperative Agreement DMR- 2128556, and in part by the State of Florida. *(Corresponding author: Yu Suetomi.)*

The authors are with the National High Magnetic Field Laboratory, Florida State University, Tallahassee, FL 32310 USA (e-mail: yu.suetomi@magnet.fsu.edu).

Color versions of one or more figures in this article are available at https://doi.org/10.1109/TASC.2025.3637739.

Digital Object Identifier 10.1109/TASC.2025.3637739

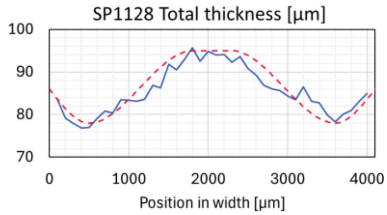

Fig. 2. Measured total thickness of the REBCO tape labeled SP1128.

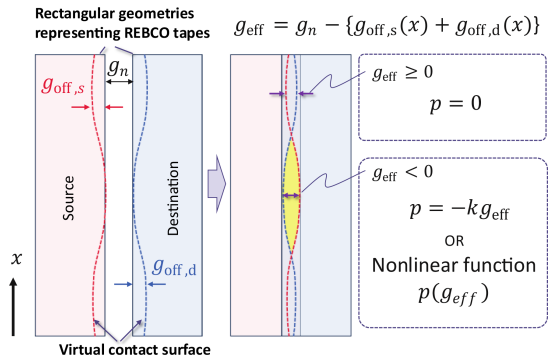

Fig. 3. Conceptual diagram of the Penalty Function with Gap Offset (PGO) method.

have been found to exhibit "needle" shape, in which the edges are thinner than the center. This is evident in the measured thickness profile of the REBCO tape labeled SP1128, as shown in Fig. 2. An optical microscopic image of the tape cross-section reveals that this variation originates from differences in the Cu layer thickness.

Such a profile is undesirable, as it creates large gaps at the tape edges within the winding pack, making it difficult to support the tape against large SCIS in the tape edge regions. Although the tape profile varies depending on the manufacturer and nominal copper thickness, it must be considered in structural analysis.

A straightforward approach to account for the thickness profile is to construct a detailed FEM geometry that explicitly represents it (detailed geometry model). However, this requires a finer mesh, leading to increased computational cost, longer simulation times, and greater difficulty in achieving convergence. As an alternative, this study introduces a method called the Penalty Function with Gap Offset (PGO).

Fig. 3 illustrates the conceptual diagram of the PGO method. In this approach, a standard rectangular geometry can be used, and the tape profile is incorporated as a gap offset distribution across the tape width within the penalty method.

In the conventional penalty method, the contact pressure p is defined as:

$$p = -kg_{\text{n}}\,(g_{\text{n}} < 0)\,,$$
$$p = 0\,(g_{\text{n}} \geq 0) \tag{1}$$

where k is the penalty factor and g_{n} is the gap distance between contact surfaces. As mentioned in the introduction, a nonlinear function $p(g_{\text{n}})$ can be used to account for the nonlinear stress–strain behavior of the winding instead of using equation (1) [8], [9]. In either case, p is computed as a function of g_{n}.

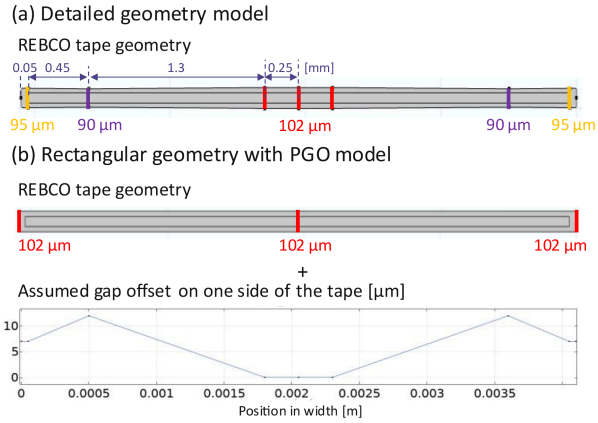

Fig. 4. (a) REBCO tape geometry for the detailed geometry model. (b) REBCO tape geometry and assumed gap offset distribution for the rectangular geometry with PGO.

In the proposed PGO method, an effective gap distance g_{eff} is introduced to incorporate the assumed gap offset, defined as:

$$g_{\text{eff}} = g_{\text{n}} - \{g_{\text{off,s}}\,(x) + g_{\text{off,d}}\,(x)\} \tag{2}$$

where x is the position along the tape width, and $g_{\text{off,s}}$ and $g_{\text{off,d}}$ are the gap offsets defined on the contact boundaries of the source and destination geometries, respectively. These offsets can be defined as functions of x. By replacing g_{n} with g_{eff}, the tape profile is effectively embedded into the contact model.

Furthermore, the tape profile affects not only the contact conditions but also the cross-sectional area of the Cu layer. To account for this, we introduce a Cu layer thickness correction factor δ, defined as:

$$\delta\,(x) = \frac{t_{\text{cu}}}{t_{\text{cu}} + g_{\text{off}}\,(x)} \tag{3}$$

where t_{cu} is the nominal Cu layer thickness, and g_{off} is the total gap offset of both tape surfaces. Using this factor, the material properties of the Cu layer are modified as follows:

$$E_r = \delta E_{cu}, E_\theta = \frac{1}{\delta}E_{cu}, E_z = \frac{1}{\delta}E_{cu} \tag{4}$$

$$\nu_{r\theta} = \delta^2\nu_{cu}, \nu_{\theta z} = \nu_{cu}, \nu_{rz} = \delta^2\nu_{cu} \tag{5}$$

$$G_{rz} = \frac{1}{\delta}G_{cu} \tag{6}$$

B. Validation Study

To validate the proposed PGO method, simulation results obtained using a rectangular geometry with the PGO model are compared with those from a detailed geometry model. Fig. 4 shows the REBCO tape geometries used in both models, and assumed gap offset distribution.

The simulation target is a small double-pancake coil consisting of 10 turns per pancake. Each turn includes two-in-hand REBCO tapes, a co-wound Cu tape and a co-wound stainless-steel tape. Detailed parameters are provided in [14]. A steady-state structural analysis is performed using Lorentz force distributions calculated from a separate electromagnetic-structural coupled model, also described in [14].

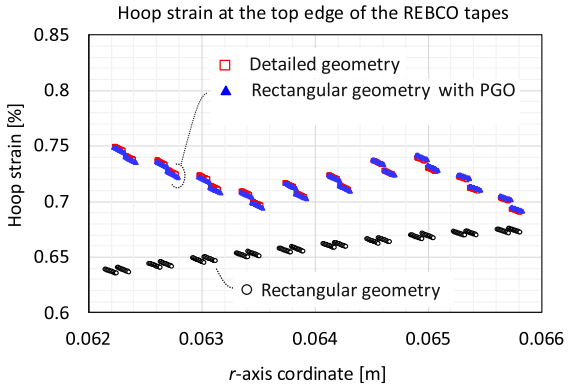

Fig. 5. Comparison of simulated hoop strain in a 10-turns double pancake coil between the detailed geometry and the rectangular geometry with PGO.

Fig. 5 presents the simulated hoop strain distribution at the top edges of the REBCO tapes. The results from the rectangular geometry with the PGO model closely match those from the detailed geometry model, demonstrating that the PGO method effectively captures the influence of the tape profile.

Additionally, both models predict larger strain values than the simple rectangular model without profile consideration. This increase is attributed to the presence of gaps between REBCO tapes caused by the non-uniform tape profile.

The results numerically validate the PGO method. Furthermore, in a separate study [15], simulation results using the PGO method were compared with experimental measurements from a large-scale coil. It was confirmed that incorporating both the REBCO tape profile and winding compressibility of over-band stainless-steel tapes—also introduced later in this paper—improved agreement with the experimental data.

III. Evaluation of Reinforcement Effectiveness With Winding Compressibility Considered

In previous work, the effectiveness of co-winding (CW) and over-banding (OB) as reinforcement options against SCIS in UHF magnets was evaluated [7]. In this study, we re-evaluate these options by taking into account both effects of non-uniform tape profile and microscopic asperities. Additionally, we assess the effectiveness of an outer ring (OR) [16], an alternative to the OB that has attracted increasing attentions. Furthermore, we investigate the influence of tape profile shape—specifically, the needle and dog-bone shapes.

A. Simulation Target

The simulation target is the end pancake disk of the outer HTS coil in the 35 T LTS/HTS hybrid magnet presented in [7]. This pancake disk consists of 130 turns of two-in-hand REBCO tapes. The detail parameters are provided in [7].

We prepared CW, OB and OR options for this disk with identical inner and outer radii and number of turns, differing only in reinforcement layout. In the CW option, reinforcement is distributed to the inside of the winding as co-wound stainless-steel tape (160 μm thick), with no over-band. In the OB option, the pancake disk includes no co-wound tape but has the over-band consisting of 100-turns stainless-steel tape (160 μm thick). Thus, the reinforcement ratio across the cross-section is identical for CW and OB. In the OR option, the over-band is replaced by a stainless-steel ring (16 mm thick). The only difference between OB and OR is the lack of contact boundaries within the reinforcement in OR.

TABLE I
Summary of Assumptions for Winding Compressibility

Contact boundary	Assumption for Non-uniform tape profile	Assumption for Microscopic roughness
RE-RE	PGO (needle or dog-bone) *	NLP $p(g_n)$ **
RE-SS	PGO (needle or dog-bone) *	NLP $p(g_n)$ **
SS-SS	-	NLP $p(g_n)$ **

RE: REBCO tape, SS: Stainless-steel tape or ring
PGO: Penalty function with gap offset, NLP: Nonlinear penalty function
*The assumed tape profiles are shown in Fig. 6 (a).
**The function is defined by eq. (8) and shown in Fig. 6 (b)

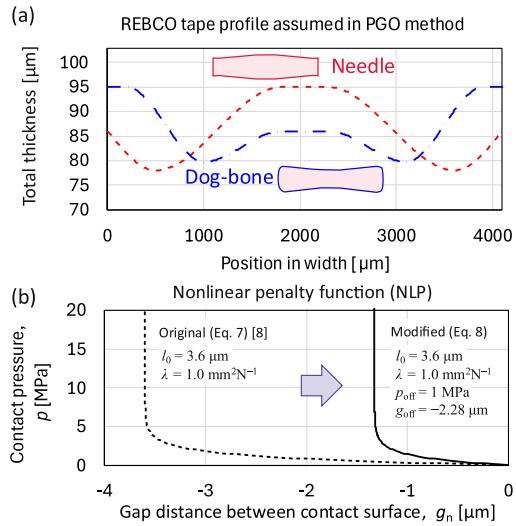

Fig. 6. (a) REBCO tape profile in PGO method, and (b) nonlinear penalty function assumed in the simulations in the section III.

B. Simulation Assumptions for Contact Boundaries

The simulation model and conditions are based on those described in [7], with modifications to the contact boundary assumptions. Table I summarizes the contact boundary conditions used in the model.

The proposed PGO method is applied to contact boundaries including the REBCO tape, labeled RE-RE and RE-SS. For boundaries between REBCO tape and stainless-steel tape or ring, labeled RE-SS, the gap offset is applied only to REBCO tape surface. The assumed tape profiles are shown in Fig. 6(a). The needle profile (red dashed line) was determined based on the measured profile shown in Fig. 2. The dog-bone profile (blue dash-dot line) was arbitrarily designed so that its edge thickness matches the center thickness of the needle profile, and its center thickness matches the edge thickness of the needle profile. Both profiles have the same cross-sectional area. In this study, these tape profiles are assumed to be uniformly distributed along the

tape length. This assumption is supported by the tape thickness measurement reported in [13], although it may depend on the manufacturer.

For considering microscopic asperities on stainless-steel tape, a nonlinear penalty function (NLP) is used:

$$p\left(g_{\mathrm{n}}\right)=-\log_e\left(\frac{g_{\mathrm{n}}}{l_0}+1\right)\Big/\lambda \tag{7}$$

where $l_0 = 3.6\ \mu$m is the initial separation at the zero contact pressure, and $\lambda = 1.0\ \mathrm{mm^2N^{-1}}$ is the compressibility characteristic. The calculated p-g_{n} curve is shown as the dashed line in fig. 6(b). The function and parameters were introduced in [8]. It should be noted that these parameters were fitted to match winding stress in pancake coils wound by a stainless-steel tape. Therefore, for stainless-steel tapes, these values are considered reasonable in the low contact pressure regime (e.g., <2 MPa), but may be inaccurate in the higher pressure regime. For microscopic asperities on REBCO tapes, parameters for fitting eq. (7) to REBCO tape winding are also introduced in [8], and Refs. [9] report the measured nonlinear stress-strain behavior of REBCO tape stacks. However, these parameters and measured data likely include the effects of non-uniform tape profiles in addition to microscopic asperities, and no data is available that isolates the nonlinear stress-strain behavior caused solely by surface asperities of REBCO tapes. Therefore, as a preliminary investigation, the parameters of eq. (7) for stainless-steel tapes are also applied to the contact boundary of REBCO tapes in this study. In future work, parameters specific to REBCO tape asperities should be investigated through surface roughness measurement and analysis.

Additionally, we introduce offset parameters g_{off} and p_{off} to consider the initial deformation caused by the winding process:

$$p\left(g_{\mathrm{n}}\right)=-\log_e\left(\frac{g_{\mathrm{n}}+g_{\mathrm{off}}}{l_0}+1\right)\Big/\lambda-p_{\mathrm{off}} \tag{8}$$

According to the winding stress measurement reported in [8], the tape-to-tape contact pressure induced by the winding process is relatively uniform in the radial direction and has a small magnitude, approximately 1 MPa, due to the effects of WCP. Therefore, we set $p_{\mathrm{off}} = 1$ MPa and $g_{\mathrm{off}} = -2.28\ \mu$m, where the value of g_{off} was determined so that the eq. (7) yields $p(g_{\mathrm{off}}) = 1$ MPa. This modified p-g_{n} curve is displayed as the solid line in fig. 6(b).

C. Simulation Procedure

The simulation procedure consists of the following steps:

1. Perform steady-state structural analysis for the cooling process without WCP assumptions.
2. Using the solutions from Step 1 as initial conditions, perform a time-stepped coupled T-A electromagnetic and structural analysis during the charging process without WCP assumptions, and obtain Lorentz force distribution at the final state.
3. Perform steady-state structural analysis for the cooling process with WCP assumptions.
4. Using the solutions from Step 3 and Lorentz force distribution from Step 2, perform steady-state structural analysis for the final state with WCP assumptions.

Winding stress is neglected in the above process. We found that the "birth and death" method, used for winding stress calculation in our model, proved unstable when WCP was considered. In this method, unwound turns are deactivated by assuming soft material properties, which leads to convergence issues under WCP conditions. As described in Section III-B, instead of conducting winding stress calculations, the initial offset values of p_{off} and g_{off} are introduced into the contact boundary conditions to account for the effects of the winding process. To perform winding stress calculations with WCP, it has been reported that solving Hakiel's winding stress model via finite difference method [8] or using a finite element model with step-by-step modeling approach [17] are effective.

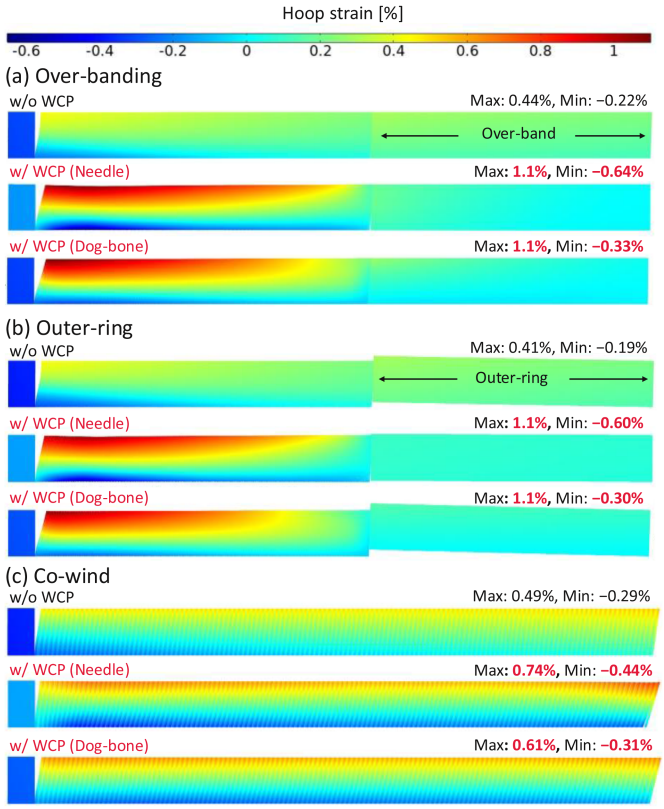

Fig. 7. Simulated hoop strain distribution of the end disk of the outer HTS coil in the 35 T LTS/HTS magnet with/without incorporating WCP—the contact boundary conditions are summarized in table I—in the case of reinforcements options of (a) over-banding, (b) outer-ring, and (c) co-winding.

D. Simulation Results

Fig. 7 compares the simulated hoop strain distributions with and without WCP, and among CW, OB, and OR options. Results with WCP are shown for both needle and dog-bone profiles. In all cases, the maximum hoop strain increases when WCP is considered.

In the OB option, the results with WCP show that strain at the outer region of the over-band is nearly zero. This is attributed to poor stress and strain transmission between stainless-steel tapes,

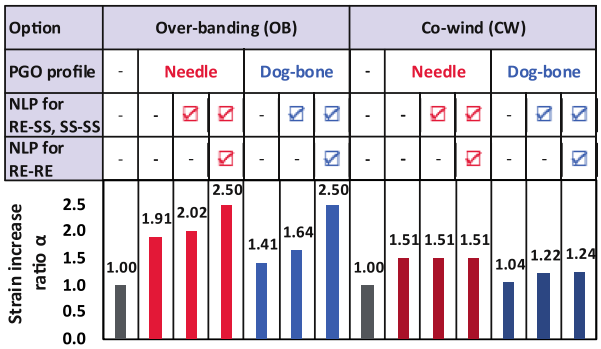

Fig. 8. Summary of contact boundary conditions and simulation results of the strain increase ratio α in each case (RE: REBCO tape, SS: Stainless-steel tape or ring, PGO: Penalty function with gap offset, NLP: Nonlinear penalty function). The symbol '-' for the PGO profile indicates that a flat profile is assumed, and the symbol '-' for NLP indicates that hard contact is assumed.

caused by WCP. This indicates that only the initial several turns of the over-band are effective, as previously pointed out in [9].

Additionally, hoop strain is concentrated in the inner winding region, particularly at the top edge of the REBCO tape. The maximum hoop strain in the REBCO tapes reaches an extremely high value of 1.1%, regardless of the assumed tape profile. This indicates that the turns in the inner region become self-supporting in both cases, due to poor stress and strain transmission between REBCO tapes. The reinforcement effect of the over-band is not effectively transmitted.

On the other hand, the magnitude of compressive hoop strain at the bottom edge of the REBCO tapes in the needle profile case is significantly greater than that in the dog-bone profile case, which may lead to buckling deformation [2], [14].

To evaluate the impact of each WCP assumption, additional simulations were performed by partially disabling the NLP assumption—i.e., by assuming "hard contact" using the standard penalty function described in Equation (1) with $k \to \infty$. Here, we introduce the strain increase ratio due to WCP, defined as:

$$\alpha = \frac{\text{Maximum hoop strain with WCP}}{\text{Maximum hoop strain without WCP}} \tag{9}$$

The simulation conditions and the resulting values of α for OB and CW options are summarized in Fig. 8. According to the α values for the OB option, the influence of microscopic asperities of the stainless-steel tape on the maximum hoop strain in the REBCO tape is not significant. Additionally, even when the REBCO tape has a dog-bone profile, the microscopic asperities cause a significant increase in hoop strain.

In the OR option, since there are no contact boundaries within the outer ring, the hoop strain is effectively distributed to the outermost region. However, hoop strain is still concentrated in the inner region for the same reasons in OB. Note that this simulation does not consider the initial radial compression introduced by the shrink-fit approach described in [16], which should be investigated in future work.

In the CW option, the strain increase ratio α is 1.51 and 1.24 for the needle and dog-bone profiles, respectively—the lowest among the three options. The distributed reinforcement via co-winding directly supports the electromagnetic forces in the REBCO tapes, without relying on stress transmission through contact boundaries. Furthermore, the results for the needle profile show a higher α value than that of the dog-bone profile, due to the presence of large gaps around the tape edges caused by its profile. Fig. 8 also indicates that, in the needle profile case, the strain increase due to WCP is primarily driven by the tape profile rather than by microscopic asperities.

As a conclusion, even if magnets are designed to keep the maximum hoop strain in REBCO tapes below 0.5% using conventional simulation models that neglect WCP, higher hoop strains may occur—particularly in the OB and OR options—potentially leading to magnet damage. Such elevated hoop strain can arise even when a REBCO tape has dog-bone profile, due to the presence of microscopic asperities. Among the three reinforcement strategies, CW is more effective than OB and OR in mitigating hoop stress and strain. However, a magnet designer should be aware of CW's drawback: its lower overall current density and reduced contribution to the central magnetic field compared to OB and OR.

Finally, it should be noted that the calculations in this study do not consider plastic deformation and I_c degradation due to strain and stress. If these effects are included, the calculated hoop strain would likely be lower [18], [19].

IV. Conclusion

In this study, we proposed a method called the Penalty Function with Gap Offset (PGO) to incorporate tape thickness profiles into FEM structural models using standard rectangular geometries. This approach models the profile as a gap offset distribution within contact boundaries.

The validity of the PGO method was confirmed by comparing simulation results with those obtained from a detailed geometry model that explicitly represents the tape profile. Furthermore, in a separate paper [15], the PGO method was shown to improve agreement between simulated and experimentally measured strain in a large-scale coil.

Using the proposed PGO method and the nonlinear penalty function to account for non-uniform tape profile and microscopic asperities, we evaluate the effectiveness of three reinforcement option: co-winding (CW), over-band (OB) and outer ring (OR), with varying needle and dog-bone tape profiles.

The results indicate that even when magnets are designed to keep the maximum hoop strain in REBCO tapes below 0.5% using conventional simulation models that neglect winding compressibility, significantly higher hoop strain may occur due to winding compressibility, potentially leading to magnet damage in any reinforcement cases. Such elevated hoop strain can arise even when a REBCO tape has dog-bone profile, due to the presence of microscopic asperities.

While OB and OR options struggle to effectively support the inner winding region due to poor stress transmission caused by winding compressibility, CW provides more direct reinforcement and is therefore more effective in mitigating hoop strain.

These findings highlight the importance of considering winding compressibility and tape profile in structural analysis and magnet design. The proposed PGO method offers a practical and accurate approach for incorporating these effects, contributing to safer and more reliable UHF magnet development.

REFERENCES

[1] Y. Li et al., "Magnetization and screening current in an 800 MHz (18.8 T) REBCO nuclear magnetic resonance insert magnet: Experimental results and numerical analysis," *Supercond. Sci. Technol.*, vol. 32, no. 10, 2019, Art. no. 105007. doi: 10.1088/1361-6668/ab3119.

[2] S. Takahashi et al., "Hoop stress modification, stress hysteresis and degradation of a REBCO coil due to the screening current under external magnetic field cycling," *IEEE Trans. Appl. Supercond.*, vol. 30, no. 4, Jun. 2020, Art. no. 4602607, doi: 10.1109/TASC.2020.2974837.

[3] Y. Yan et al., "Screening current effect on the stress and strain distribution in REBCO high-field magnets: Experimental verification and numerical analysis," *Supercond. Sci. Technol.*, vol. 33, no. 5, 2020, Art. no. 05LT02, doi: 10.1088/1361-6668/ab7c52.

[4] H. Ueda et al., "Experiment and numerical simulation of the combined effect of winding, cool-down, and screening current induced stresses in REBCO coils," *Supercond. Sci. Technol.*, vol. 35, no. 5, 2022, Art. no. 054001, doi: 10.1088/1361-6668/ac4b9e.

[5] D. J. Kolb-bond et al., "Computing strains due to screening currents in REBCO magnets," *IEEE Trans. Appl. Supercond.*, vol. 30, no. 4, Jun. 2020, Art. no. 4602805.

[6] D. Kolb-Bond et al., "Screening current rotation effects: SCIF and strain in REBCO magnets," *Supercond. Sci. Technol.*, vol. 34, no. 9, 2021, Art. no. 095004, doi: 10.1088/1361-6668/ac1525.

[7] Y. Suetomi et al., "Screening current induced stress/strain analysis of high field REBCO coils with co-winding or over-banding reinforcement," *IEEE Trans. Appl. Supercond.*, vol. 34, no. 5, Aug. 2024, Art. no. 8400206.

[8] Y. Yan et al., "Measurement and analysis of winding stresses in dry-wound pancake coils considering nonlinear compressive behaviors," *Supercond. Sci. Technol.*, vol. 36, no. 11, 2023, Art. no. 115019.

[9] J. Park et al., "Numerical study on effect of boundary conditions and winding compressibility on screening current induced stress," *IEEE Trans. Appl. Supercond.*, vol. 35, no. 5, Aug. 2025, Art. no. 4801805.

[10] S. Xue, J. Kwon, Y. Guo, T. Garg, M. D. Sumption, and E. W. Collings, "Compressive stress-strain behavior of REBCO coated conductors and cables," *IEEE Trans. Appl. Supercond.*, vol. 33, no. 5, Aug. 2023, Art. no. 4800706.

[11] S. Ryu, C. Lee, Y. Choi, K. Sim, S. Hahn, and S. Kim, "Deformation behavior of stacked REBCO tapes under compressive loads," *IEEE Trans. Appl. Supercond.*, vol. 34, no. 5, Aug. 2024, Art. no. 6602305.

[12] J. Park, J. Kim, Y. Yan, and S. Hahn, "Diameter change of dry wound REBCO solenoid pancake coil by winding tension," *IEEE Trans. Appl. Supercond.*, vol. 34, no. 5, Aug. 2024, Art. no. 8400605.

[13] I. Park, G. Kim, H. Kim, J. Kim, and H. Ha, "Development of continuous thickness measurement system for long-length HTS CCs," *IEEE Trans. Appl. Supercond.*, vol. 35, no. 5, Aug. 2025, Art. no. 6603305, doi: 10.1109/TASC.2025.3532238.

[14] Y. Suetomi, K. Kim, T. Adkins, H. Bai, and I. R. Dixon, "Combined axial pressure and screening current induced stress test on REBCO pancake coils," *IEEE Trans. Appl. Supercond.*, vol. 35, no. 5, Aug. 2025, Art. no. 4600807, doi: 10.1109/TASC.2024.3520943.

[15] S. Griffin et al., "Measured and simulated strain in the large scale coil with considering winding compressibility," *IEEE Trans. Appl. Supercond.*, vol. 36, no. 5, Aug. 2025, Art. no. 4601805.

[16] B. Bordini et al., "Conceptual design of a ReBCO non/metal-insulated ultra-high field solenoid for the Muon collider," *IEEE Trans. Appl. Supercond.*, vol. 34, no. 3, May 2024, Art. no. 4301310.

[17] L. Zhihua et al., "Finite element approach for calculating stress distribution in non-circular high-temperature superconducting coils," *Superconductivity*, vol. 14, pp. 2772–8307, 2025.

[18] J. Bang et al., "Elastic-plastic conductor damage evaluation at over 0.4% strain using a high-stress REBCO coil," *Supercond. Sci. Technol.*, vol. 37, 2024, Art. no. 095011.

[19] Y. Yan et al., "Electromagnetic-mechanical simulation of high-field test coils and conductor degradation," *IEEE Trans. Appl. Supercond.*, vol. 34, no. 5, Aug. 2024, Art. no. 4602605.